http://dx.doi.org/10.5012/bkcs.2013.34.5.1481

Bifunctional Fe-SBA-15-SO$_3$H Mesoporous Catalysts with Different Si/Fe Molar Ratios: Synthesis, Characterization and Catalytic Activity

Sezer Erdem,[*] Beyhan Erdem,[†,*] Ramis Mustafa Öksüzoğlu,[‡] and Alime Çıtak[§]

Department of Physics, Faculty of Science and Arts, Uludag University, 16059 Bursa, Turkey. [*]E-mail: serdem@uludag.edu.tr
[†]Department of Chemistry, Faculty of Science and Arts, Uludag University, 16059 Bursa, Turkey
[*]E-mail: gbeyhan@uludag.edu.tr
[‡]Department of Material Science and Engineering, Faculty of Engineering, Anadolu University, 26470 Eskisehir, Turkey
[§]Department of Chemical Engineering, Eskisehir Osmangazi University, 26480 Eskisehir, Turkey
Received December 27, 2012, Accepted February 25, 2013

Bifunctional Fe-SBA-15-SO$_3$H mesoporous materials with different Si/Fe molar ratios (3, 5, and 7) have been synthesized *via* a simple direct hydrothermal method and characterized by XRD, N_2-adsorption/desorption, TG/DTG and FT-IR techniques, and used as solid acid catalysts in the esterification of lactic acid with methanol. XRD and N_2 sorption characterizations show successful iron doping within the mesoporous channels of SBA-15-SO$_3$H. The FT-IR and TG/DTG characterizations also reveal the presence of iron. With the incorporation of Fe ions into the SBA-15-SO$_3$H, the acid sites substantially increased because of the self-separated acidity of the hydrolysis of Fe^{3+} solutions. However, in the Si/Fe = 3 molar ratio, the catalytic conversion decreased which is caused by the reduced cooperation effect between the acid pairs due to the weakened hydrogen bonds and collapse of the pore structure. This further suggests that the mesoporous structure decreases with the decrease in Si/Fe ratio.

Key Words : Esterification, Lactic acid, Fe-SBA-15-SO$_3$H, Mesoporous catalysts

Introduction

Mesoporous silicas have increasingly attached attention since the development of the M41S family due to their highly tailorable properties such as pore size, surface area, pore volume and well-ordered structure.[1] SBA-15 is by far a large scale pore-size mesoporous material with highly ordered hexagonally arranged meso-channels, with thick walls, adjustable pore size from 3 to 30 nm, and high hydrothermal and thermal stability.[2] Furthermore, the synthesis of SBA-15 can be accomplished using a cheap silica source, which makes this synthesis commercially viable.[3,4] These special features lead to interesting applications in catalysis, separation technology, optoelectronics, and adsorption.[1] However, pure silica SBA-15 mesoporous materials possess neutral Si frameworks which limit their broad applicability. Therefore, it is of great importance to introduce active sites in the mesopore frameworks. So far, various kinds of metal ions and nitrogen atoms substituted SBA-15 mesoporous powders and thin films have been prepared.[5-13] In particular, their large pore size makes the nanoparticles-incorporated SBA-15 attractive as catalysts for reactions. These nano-sized particles increase the exposed surface area of the active component of the catalyst, accordingly the contact between reactants and catalyst increases dramatically like in homogeneous catalysts. Moreover, the incorporation of metal ions into the mesoporous materials leads to additional different Bronsted acidity, which is required for acid catalyzed reactions. Unfortunately, the synthesis condition of SBA-15 is acidic, and therefore, it is difficult to embed the nanoparticles. Consequently, the amount of nanoparticles incorporated into the framework of mesoporous materials is very low.[14,15] However, metal ions are generally in an isolated state in acidic solution, whereas they easily precipitate from solution to form metal oxides in basic solution. Therefore, metal ions should be more highly dispersed in the metal-substituted mesoporous materials prepared under acidic conditions than in those prepared under basic conditions. Thus, although Fe-zeolites and Fe-MCM-41 prepared in basic media have been widely investigated, the incorporation of Fe into the framework of SBA-15 by simple direct hydrothermal methods prepared in acidic media has rarely been reported.[16]

Esterification of carboxylic acids with alcohols represents a well-known category of liquid-phase reactions of considerable industrial interest due to the enormous practical importance of organic ester products. These ester products include environmentally friendly solvents, flavours, pharmaceuticals, plasticizers, polymerization monomers and emulsifiers in the food, cosmetic and chemical industries.[17] The selection of lactic acid as esterfication substrate has following major reasons: on one hand due to its occurrence in nature is widespread, and its utility as a monomer for biodegradable polymers, and on the other hand, it can be produced from fermentation of carbohydrate materials at low cost. Lactic acid is oligomerized at high concentration to the lactylactic acid because of two functional groups in the lactic acid molecule and the vapour pressure of lactic acid is very low (14 mmHg at 122 °C). Therefore, normal distillation is not applicable to the purification of lactic acid. In

order to solve these purification problems, the esterification of lactic acid with alcohol, distillation of produced volatile ester, and reverse reaction of ester to purified lactic acid have been studied.[18-20] Conversions for the esterification reactions have long been known to be limited by a slow reaction rate and the existence of reversible reactions. To accelerate the reaction rate, catalysts are always employed in a liquid-phase esterification. Despite the strong catalytic effect, the use of homogeneous catalysts, such as sulfuric acid and *p*-toluene sulfonic acid suffers from several drawbacks, such as the existence of side reactions, corrosion of the equipment and the need to deal with acidic wastes. Under this situation, the use of solid acid catalyst has received great attention due to its distinct advantages, such as the higher purity of the products and easily removing of catalyst from the reaction mixture. However, some critical factors such as the activity, stability, availability, and the cost of the catalyst and the short development time for a production process are probably most decisive.[21] From this point of view, sulfonic acid functionalized heterogeneous acid catalysts are the predominant materials. Especially mesoporous silicas functionalized by propyl sulfonic groups are developed for a high accessibility of the single site and concentrated acid strength, which are promising catalyst for variety of reactions such as esterification, etherification and condensation reactions.[22-24] To our best knowledge, sulfonic acid group[25-29] and Fe substituted SBA-15[30] are studied separately very often.

In the present study, both propyl-sulfonic acid group and Fe functionalized SBA-15 mesoporous catalysts were synthesized and the activity of these materials has been compared to that of SBA-15-SO_3H "single site". It has been found that, SBA-15-SO_3H with "single site" is an effective acid catalyst alone and the incorporation of Fe into the material leads to higher acidity, but the accessibility of acid sites of Fe-SBA-15-SO_3H is hindered because of the collapse of the mesostructure with high Fe loading.

Experimental

The Fe-SBA-15-SO_3H mesostructure catalysts were prepared from tetraethylorthosilicate (TEOS) as the silica source under acidic conditions using a triblock copolymer poly(ethylene glycol)-block-poly(propylene glycol)-block-poly(ethylene glycol) (Pluronic P123) as a structure directing agent by following the published procedure.[31] The mesoporous silicas were modified with MPTMS and $Fe(NO_3)_3{\cdot}9H_2O$ as organosilica and Fe source, respectively. In a typical synthesis, 4 g of P123 was added to 97.58 g of water. After stirring 2 h, a clear solution was obtained, then 1.97 g of 37 wt % aqueous HCl (Merck) was added to the solution with vigorous stirring. After completing dissolution, the solution was heated to 40 °C. In each experiment, 7.69 g of TEOS and the required amount of $Fe(NO_3)_3{\cdot}9H_2O$ were added for prehydrolysis for 2 h. Then 0.81 g MPTMS and 8.37 g of H_2O_2 were added dropwise. The resulting mixture was stirred for 24 h at 40 °C followed by aging from 100 °C for another 24 h under static conditions. The molar composition of the mixture for 4 g P123 was 1TEOS:0.1MPTMS:0.54HCl:$6.31H_2O$:$1.8H_2O_2$:X$Fe(NO_3)_3{\cdot}9H_2O$, where X = 0.0053 (the mol ratio of Si/Fe = 7), 0.0074 (Si/Fe = 5), and 0.0123 (Si/Fe = 3). The template was removed from the as-synthesized material by washing with ethanol under reflux for 24 h. The samples were prepared by changing the molar Si/Fe ratios and defined as Fe-SBA-15-SO_3H(Y), where Y denoted the molar Si/Fe ratio of the samples. Pure SBA-15-SO_3H, herein, was also prepared for the comparison purpose.

Low and high angle X-ray powder diffraction (XRD) patterns were collected on a Bruker D8 Advance diffractometer using Cu-Kα radiation. Typically, the data were collected from 0.4 to 3° (2θ) and from 30 to 40° (2θ) for low and high angle XRD, respectively. Nitrogen sorption isotherms were measured at 77 K with Quantachrome, Autosorb 1C sorption analyzer. Before the measurements, the samples were degassed at 200 °C in vacuum for 5 h. A Thermo Nicolet 6700 series infrared spectrometer was used for FT-IR analysis in normal transmission mode with a KBr detector over the range of 4000-400 cm^{-1} at a resolution of 8 cm^{-1} averaged over 32 scans. Thermogravimetric analyses were performed with a SII-EXSTAR TG/DTA 6200 system. The samples (~5-10 mg) were heated from room temperature to 800 °C under dried-air atmosphere at a scanning rate of 10 °C/min. The acid exchange capacities of the Fe-SBA-15-SO_3H(Y) and pure SBA-15-SO_3H were measured by means of titration, using sodium chloride as exchange agent. In a typical experiment, 0.05 g of solid was added to 10 g of aqueous solution of sodium chloride (2 M). The resulting suspension was allowed to equilibrate and thereafter titrated potentiometrically by drop-wise addition of 0.01 M NaOH (aq).[28,32]

Esterification runs were performed at 333 K in a stirred batch reactor equipped with a heating jacket. The reaction temperature was controlled within ± 0.1 K by circulating water from a thermostat into a cylindrical water-jacketed reactor. In order to monitor the reaction, the samples were withdrawn periodically at time intervals ranging from 0 to 6 h. When the esterification reaction is carried out at high lactic acid concentration, polylactic acid is formed due to self-esterification.[33] Therefore, dilute aqueous solution of lactic acid (20% by mass) was used in order to avoid the formation of polymers. Typically, the molar composition of the reaction mixture was: 0.05 mol of lactic acid (which acts also as solvent), 0.15 mol methanol and a catalyst loading of 0.5 g (2 wt %). The concentration of lactic acid was determined by titration using standardized 0.1 N NaOH solutions.

Results and Discussion

Powder X-ray diffraction has been used to assess the structural ordering of the pure SBA-15-SO_3H and Fe-SBA-15-SO_3H(3) materials. Figure 1(a) shows the low angle powder X-ray diffraction patterns of pure SBA-15-SO_3H and Fe-SBA-15-SO_3H(3) (inset picture). In the same figure, XRD patterns of used forms of these materials are also

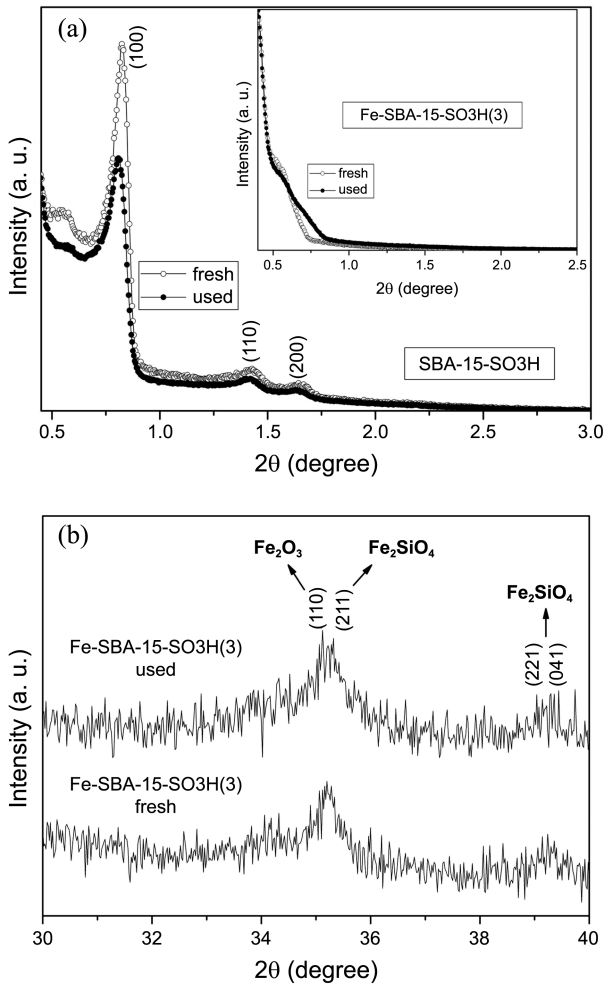

Figure 1. (a) Low angle XRD patterns of the SBA-15-SO$_3$H and Fe-SBA-15-SO$_3$H(3), (b) high angle XRD patterns of the Fe-SBA-15-SO$_3$H(3) materials in fresh and used forms.

shown. Low angle XRD patterns for pure SBA-15-SO$_3$H reveal three well-ordered peaks (100), (110) and (200), which are characteristic of mesoporous material with 2D-hexagonal structure. In contrast to that, low angle XRD patterns of fresh and used Fe-SBA-15-SO$_3$H(3) materials (the inset picture of Figure 1(a)), do not show the hexagonal mesoporous structure, indicating a collapse of the pore structure with high Fe loading.[31] The reduction of the diffraction intensities of the (100) XRD peaks in Figure 1(a) is attributable to the increasing destructive interferences by filling the pores with rising amount of the iron oxide nanoparticles. In general, the introduction of scattering material into the pores leads to an increased phase cancellation between scattering from the wall and the pore regions and therefore to reduced scattering intensities for the Bragg reflection.[34] When the silica species and iron species co-existed in the aqueous solutions with pH values lower than 2.0 (~isoelectric point of silica), the main iron species are Fe^{3+} ions. The formation of iron oxide is impossible at high acidic conditions because of the difficulties in the formation of metal-O-Si bonds under the strong acidic condition. Only when the iron concentration reaches a certain high value (for the sample with Si/Fe ratio equal to 3), can the extra framework iron clusters and iron oxides be formed.[16] In addition, samples with Si/Fe molar ratios between 7 and 5 are white, indicating that the amount of iron oxide formed in the Fe-SBA-15-SO$_3$H samples is very low or highly isolated. When Si/Fe molar ratio is 3, the sample is brown, indicating that iron oxides are formed. In order to clarify the existence of iron oxide nanoparticles, the high angle diffraction patterns of Fe-SBA-15-SO$_3$H(3) have been taken (Figure 1(b)), and the measurements confirm the coexistence of hexagonal hematite (Fe_2O_3) and orthorhombic fayelite (Fe_2SiO_4). Hematite is extremely stable at ambient conditions, and often is the end product of the transformation of other iron oxides.[35] In water, arrays of hematite nanorods have been obtained by pH adjustments. At very low pH, the hydrolysis-condensation of iron species barely occurs, and high ionic strength yields to the formation of highly charged anisotropic particles. Indeed, the main diffraction peak, (211), of fayelite phase overlaps with that of the hematite (110) peak, and an inversion in the relative intensities of the hematite diffraction peaks is observed when crystalline fayelite is present in large proportion.[36] In order to check the structural ordering of SBA-15-SO$_3$H and Fe-SBA-15-SO$_3$H(3) after catalytic cycle, the XRD patterns of the spent catalyst were recorded and presented in Figure 1(a) and 1(b) along with that of fresh catalyst for comparison purposes. The intensities of peaks of used catalysts are found to be comparatively same as that of fresh catalyst indicating the stability of the materials.[37]

Figure 2 shows the N_2 adsorption/desorption isotherms and pore size distributions of the samples. The N_2 adsorption/desorption isotherms of all samples indicated that there

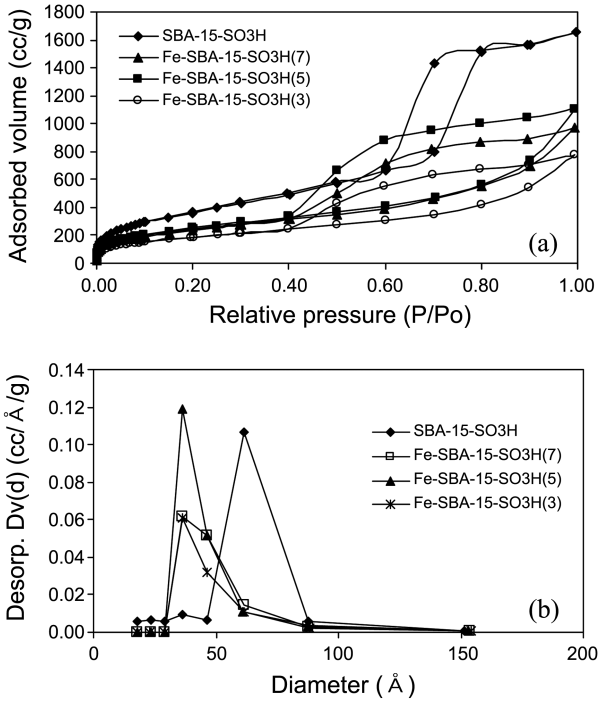

Figure 2. (a) Nitrogen sorption isotherms, (b) pore size distributions of the SBA-15-SO$_3$H and Fe-SBA-15-SO$_3$H(Y) samples.

are type IV isotherms with a H1-type loop resulting from a capillary condensation taking place in mesopores. A slight hysteresis loop and sharp adsorption step at relative pressures around 0.4-0.6 identify the characteristics of this isotherm[38,39] and the sharpness of the adsorption branches indicates narrow pore size distribution.[40] In Figure 2(a), the slope of the isotherm after the low-pressure adsorption step is lower for Fe loaded SBA-15-SO_3H than that of pure SBA-15-SO_3H, corresponding to a lower area of the mesopore surface.[41] Fe-SBA-15-SO_3H exhibited a slight condensation step, being indicative of a change of hexagonal structure, which is in agreement with the results of XRD. Furthermore, the capillary condensation step shifted to higher relative pressures with loading of Fe in the samples (Figure 2(a)) and the BJH pore size distributions broadened (Figure 2(b)). This further suggests that the mesoporous structure decreased with the decrease in Si/Fe ratio.[31]

The results for surface area, pore size and pore volume are presented in Table 1. When Fe was loaded to SBA-15-SO_3H, the accessible porous volume and specific surface area decreased relative to the support, SBA-15-SO_3H. For example, mesopore size changes from 8.12 to 7.05 nm (13%) for SBA-15-SO_3H and Fe-SBA-15-SO_3H(3) and mesopore volume decreases from 2.57 to 1.21 (53%). But this is not enough to prove that iron oxide particles have grown inside the pores. Indeed, large oxide particles generated on the outlet of silica grains can also plug the mesopore entrance.[42] However, three independent observations confirm that some of the iron oxide particles are located inside the pores: 1) For a given iron amount, the specific surface area decrease follows the structural parameters of the silica hard template. 2) The diameter of the mesopores obtained by applying the BJH formulas to the desorption branch of the isotherm decreases after iron introduction. 3) The hysteresis loop becomes broader as suggested by Delahaye *et al*.[43]

Figure 3 shows the FT-IR spectra of SBA-15-SO_3H, Fe-SBA-15-SO_3H(7), Fe-SBA-15-SO_3H(5), and Fe-SBA-15-SO_3H(3), respectively. The characteristic absorption peaks of SBA-15-SO_3H are evident at 450 cm^{-1} (SiO_4, tetrahedron vibration), at 800 cm^{-1} (Si-O-Si, symmetric vibration) and 2935 cm^{-1} (C-H stretching vibration of propyl chain), respectively. O-H stretching vibration due to physorbed water and potentially surface hydroxyls near 3420 cm^{-1}, and O-H deformation vibration near 1630 cm^{-1} could be seen in the all of the samples. The introduction of Fe into the SBA-15-SO_3H was confirmed by the band around at 600 cm^{-1} assigned to the Fe-O absorption band.[44] It is noteworthy from

Table 1. Textural and acidic properties of pure and Fe loaded SBA-15-SO_3H samples

Sample	S_{BET} (m^2/g)	V_{pore} (cm^3/g)	d_{pore} (nm)	H^+ (meq/g)
SBA-15-SO_3H	1265	2.57	8.12	0.95
Fe-SBA-15-SO_3H(7)	838	1.50	6.84	1.02
Fe-SBA-15-SO_3H(5)	848	1.71	7.90	1.19
Fe-SBA-15-SO_3H(3)	633	1.21	7.05	1.43

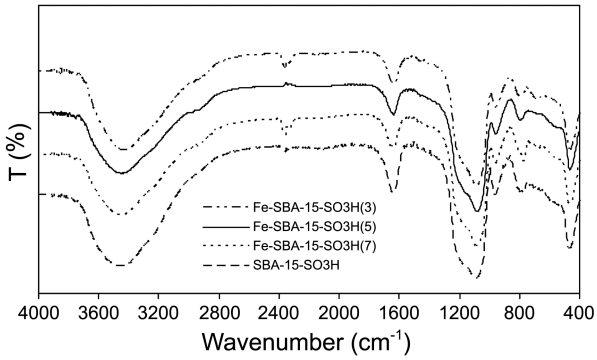

Figure 3. FT-IR spectra of the SBA-15-SO_3H and Fe-SBA-15-SO_3H(Y) samples.

Figure 3 that the intensity of the bands found in pure SBA-15-SO_3H material significantly decreases with increasing Fe loading.

Figure 4 shows the thermal analyses of pure SBA-15-SO_3H and Fe-SBA-15-SO_3H(3). Since the boulders of the TG curve at around 500 °C can hardly be seen, the corresponding temperatures are difficult to determine, and it can be performed more readily by using the DTG curve which shows the rate of mass change with respect to temperature. For pure SBA-15-SO_3H (Figure 4(a)), the exponential weight decay until 100 °C in TG and the first peak in DTG can be attributed to the removal of physisorbed water. A remarkable weight loss around 500 °C in TG and the second peak in DTG analyses indicate thermal decomposition of the

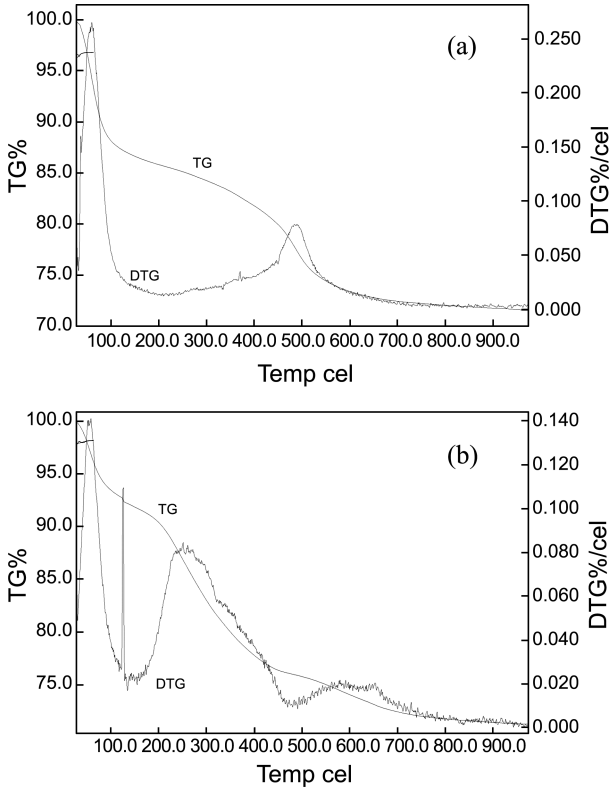

Figure 4. (a) TG/DTG curves for (a) SBA-15-SO_3H, (b) Fe-SBA-15-SO_3H(3).

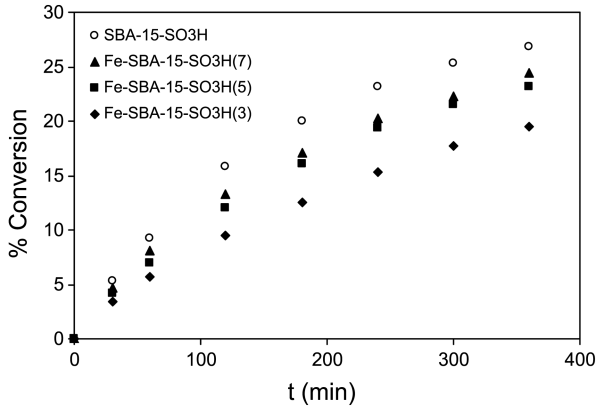

Figure 5. % Conversion of lactic acid in the presence of pure SBA-15-SO$_3$H and Fe-SBA-15-SO$_3$H(Y) catalysts.

SBA-15-SO$_3$H. Although the difference between the TG curves of pure and Fe loaded SBA-15-SO$_3$H (Figure 4(b)) can not be discerned clearly, in the DTG curve of Fe-SBA-15-SO$_3$H(3) four peaks can be seen compared to SBA-15-SO$_3$H. The first and the second peaks in DTG curve of Fe-SBA-15-SO$_3$H(3) assign the removal of physisorbed and interlayer physisorbed water, the third peak assigns the weakly bound Fe-SBA-15-SO$_3$H(3) and the last peak around 600 ^{o}C assigns the strongly bound Fe-SBA-15-SO$_3$H, respectively. This broad exothermic peak relates to the phase transformation.[45]

Since the acidic sites in materials are critical for the esterification reaction, the number of acid sites has been determined by means of acid-base titration and the results are summarized in Table 1. The improved acidity in the presence of Fe^{3+} ions reveals that the Fe^{3+} may take the place of protons and participate in the self-assembly process.[16]

Figure 5 illustrates the catalytic performance of SBA-15 modified by sulfonic group and Fe with varying Si/Fe molar ratio in the synthesis of methyl lactate. Indeed, catalytic activity and product selectivity are strongly dependent on the amount of Bronsted acid sites. However, the activity was also related to the mesoporous structure. As the Fe content of SBA-15-SO$_3$H increased (Table 1), Bronsted acidity increased but the molar yield of the ester decreased (Figure 5). The difference between the catalytic performance and acid strength of the organosulfonic acid and Fe functionalized mesoporous catalyst suggests that the additional factors beyond acid strength can affect the ultimate performance of the acid solid catalyst. A possible explanation for the discrepancy between the acid strength and catalytic activity for Fe-SBA-15-SO$_3$H in proximity could be a decreased cooperation effect between the acid pairs due to the weakened hydrogen bonds since it is proposed that the Fe^{3+} may take the place of protons and participate in the self-assembly process.[16,46]

Conclusion

In conclusion, SBA-15-SO$_3$H and Fe-SBA-15-SO$_3$H mesoporous catalysts with different Si/Fe molar ratios have been synthesized by using a direct hydrothermal route. The samples have been examined by XRD, N_2 adsorption/desorption, TG/DTG and FT-IR methods and used as catalysts in the esterification of lactic acid with methanol. Kinetic and characterization investigations indicate that the materials contain a variety of acid sites whose contents vary in a systematic manner with Si/Fe molar ratio of the materials. That is: as the incorporation of Fe into the SBA-15-SO$_3$H increases, the acid sites substantially increase because of the H^+ produced by the hydrolysis of Fe^{3+} in water. With low iron concentrations (Si/Fe molar ratio between 5 and 7) and at strongly acidic conditions, the main form of iron species existed in the solution is Fe^{3+} cations. For this reason, when the molar ratio is about 7 or 5, reaction conversion has been changed slightly. However, when the Si/Fe molar ratio equals to 3, the catalytic conversion decreased which is caused by the decreased cooperation effect between the acid pairs due to the weakened hydrogen bonds and collapse of high Fe amount in the mesopore. It can be concluded from the results that when the iron concentration reaches a certain high value, metal oxides tend to appear in the channel or external surface of the products as by products which would jam the channels or play a negative role in catalysis, even if the reaction condition is highly acidic.

Acknowledgments. This work was supported by The Commission of Scientific Research Projects of Uludag University, Project number: UAP(F)-2011/69. And the publication cost of this paper was supported by the Korean Chemical Society.

References

1. Gobin, O. C.; Wan, Y.; Zhao, D.; Kleitz, F.; Kaliaguine, S. *J. Phys. Chem. C* **2007**, *111*, 3053.
2. Zheng, X.; Dong, B.; Yuan, C.; Zhang, K.; Wang, X. *J. Porous Mater.* **2012**, DOI 10.1007/s10934-012-9626-6.
3. Kim, J. M.; Stucky, G. D. *Chem. Commun.* **2000**, 1159.
4. Kim, S. S.; Karkamkar, A.; Pinnavaia, T. J.; Kruk, M.; Jaroniec, M. *J. Phys. Chem. B* **2001**, *105*, 7663.
5. Newalkar, B. L.; Olanrewaju, J.; Komarneni, S. *J. Phys. Chem. B* **2001**, *105*, 8356.
6. Dong, X.; Shen, W.; Zhu, Y.; Xiong, L.; Shi, J. *Adv. Funct. Mater.* **2005**, *15*, 955.
7. Sauer, J.; Marlow, F.; Spliethoff, B.; Schüth, F. *Chem. Mater.* **2002**, *14*, 217.
8. Karimi, Z.; Mahjoub, A. R. *Appl. Surf. Sci.* **2010**, *256*, 4473.
9. Shukla, P.; Wang, S.; Sun, H.; Ang, H. M.; Tade, M. *Chem. Eng. J.* **2010**, *164*, 255.
10. Zhang, X.; Yuan, C.; Li, M.; Gao, B.; Wang, X.; Zheng, X. *J. Non-Cryst. Solids* **2009**, *355*, 2209.
11. Nozaki, C.; Lugmair, C. G.; Bell, A. T.; Tilley, T. D. *J. Am. Chem. Soc.* **2002**, *124*, 13194.
12. Li, Y.; Zhang, W.; Zhang, L.; Yang, Q.; Wei, Z.; Feng, Z.; Li, C. *J. Phys. Chem. B* **2004**, *108*, 9739.
13. Xiu, T.; Liu, Q.; Wang, J. *J. Mater. Res.* **2007**, *22*, 1834.
14. Liu, C. Y.; Chen, C. F.; Leu, J. P.; Lin, Y. C. *J. Sol-Gel Sci. Techn.* **2007**, *43*, 47.
15. Polshettiwar, V.; Varma, R. S. *Green Chem.* **2010**, *12*, 743.
16. Li, Y.; Feng, Z.; Lian, Y.; Sun, K.; Zhang, L.; Jia, G.; Yang, Q.; Li,

C. *Micro. Meso. Mater.* **2005**, *84*, 41.
17. Liu, Y.; Lotero, E.; Goodwin, J. G. *J. Mol. Catal. A: Chem.* **2006**, *245*, 132.
18. Choi, J. I.; Hong, W. H.; Chang, H. N. *Int. J. Chem. Kinet*. **1996**, *28*, 37.
19. Sanz, M. T.; Murga, R.; Beltran, S.; Cabezas, J. L.; Coca, J. *Ind. Eng. Chem. Res*. **2002**, *41*, 512.
20. Sanz, M. T.; Murga, R.; Beltran, S.; Cabezas, J. L.; Coca, J. *Ind. Eng. Chem. Res*. **2004**, *43*, 2049.
21. Erdem, B.; Kara, A. *React. Funct. Polym.* **2011**, *71*, 219.
22. Zhu, H.; Shanks, B. H.; Heindel, T. J. *Ind. Eng. Chem. Res.* **2008**, *47*, 7881.
23. Lai, D.; Deng, L.; Li, J.; Liao, B.; Guo, Q.; Fu, Y. *ChemSusChem* **2011**, *4*, 55.
24. Van Rhijn, W. M.; De Vos, D. E.; Sels, B. F.; Bossaert, W. D.; Jacobs, P. A. *Chem. Commun.* **1998**, 317.
25. Kureshy, R. I.; Ahmad, I.; Pathak, K.; Khan, N. H.; Abdi, S. H. R.; Jasra, R. V. *Catal. Commun.* **2009**, *10*, 572.
26. Jackson, M. A.; Appell, M. *Appl. Catal. A: Gen.* **2010**, *373*, 90.
27. Shen, J. G. C.; Herman, R. G.; Klier, K. *J. Phys. Chem. B* **2002**, *106*, 9975.
28. Margolese, D.; Melero, J. A.; Christiansen, S. C.; Chmelka, B. F.; Stucky, G. D. *Chem. Mater.* **2000**, *12*, 2448.
29. Hermida, L.; Abdullah, A. Z.; Mohamed, A. R. *J. Porous Mater.* **2012**, *19*, 835.
30. Mayani, S. V.; Mayani, V. J.; Kim, S. W. *Bull. Korean Chem. Soc.* **2012**, *33*, 3009.
31. Zheng, Y.; Li, J.; Zhao, N.; Wei, W.; Sun, Y. *Micro. Meso. Mater.* **2006**, *92*, 195.
32. Çıtak, A.; Erdem, B.; Erdem, S.; Öksüzoğlu, R. M. *J. Colloid Interface Sci.* **2012**, *369*, 160.
33. Yixin, Q.; Shaojun, P.; Shui, W.; Zhiqiang, Z.; Jidong, W. *Chin. J. Chem. Eng.* **2009**, *17*, 773.
34. Lim, M. H.; Blanford, C. F.; Stein, A. *Chem. Mater.* **1998**, *10*, 467.
35. Teja, A. S.; Koh, P. Y. *Prog. Cryst. Growth Charact. Mater.* **2009**, *55*, 22.
36. Cornu, C.; Bonardet, J. L.; Casale, S.; Davidson, A.; Abramson, S.; Andre, G.; Porcher, F.; Grcic, I.; Tomasic, V.; Vujevic, D.; Koprivanac, N. *J. Phys. Chem. C* **2012**, *116*, 3437.
37. Eswaramoorthi, I.; Dalai, A. K. *Int. J. Hydrogen Energy* **2009**, *34*, 2580.
38. Shi, X.; Wu, Y.; Yi, H.; Rui, G.; Li, P.; Yang, M.; Wang, G. *Energies* **2011**, *4*, 669.
39. Sing, K. S. W. *Pure Appl. Chem.* **1982**, *54*, 2201.
40. Grieken, R. V.; Calleja, G.; Stucky, G. D.; Melero, J. A.; Garcia, R. A.; Iglesias, J. *Langmuir* **2003**, *19*, 3966.
41. Zhao, D.; Huo, Q.; Feng, J.; Chmelka, B. F.; Stucky, G. D. *J. Am. Chem. Soc.* **1998**, *120*, 6024.
42. Khodakov, A. Y.; Bechara, R.; Griboval-Constant, A. *Appl. Catal. A: Gen.* **2003**, *254*, 273.
43. Delahaye, E.; Escax, V.; El Hassan, N.; Davidson, A.; Aquino, R.; Dupuis, V.; Perzynski, R.; Raikher, Y. L. *J. Phys. Chem. B* **2006**, *110*, 26001.
44. Mu, B.; Wang, T.; Wu, Z.; Shi, H.; Xue, D.; Liu, P. *Colloids Surf. A: Physicochem. Eng. Aspects* **2011**, *375*, 163.
45. Gu, M.; Yue, B.; Bao, R.; He, H. *Mater. Res. Bull.* **2009**, *44*, 1422.
46. Mbaraka, I. K.; Shanks, B. H. *J. Catal.* **2006**, *244*, 78.